Supplement of Geosci. Model Dev., 18, 6023–6041, 2025
https://doi.org/10.5194/gmd-18-6023-2025-supplement

Geoscientific Model Development
Open Access
EGU

Supplement of

REtrieval Method for optical and physical Aerosol Properties in the stratosphere (REMAPv1)

Andrin Jö et al.

Correspondence to: Andrin Jörimann (andrin.joerimann@pmodwrc.ch)

Supplement

S1 Method for the 50 year record

This section contains additional information on the retrieval method used for the SAGE-3λ and SAGE-4λ records. The method is generally analogous to the retrieval described in the main text, with the differences and parameterizations specific to certain time periods recorded here.

This paper includes a whole 50 year data record (1960 – 2011), termed SAGE-3λ which chiefly utilizes three of the four SAGE II wavelengths (3λ), besides some other satellite extinction coefficients, plus information from tropical ground-based LIDARs for the filling of data gaps under volcanically opaque conditions. For parts of this period only limited information is available, e.g. aerosol extinction coefficients (AEC) only at a single wavelength (as is the case for data from SAGE, SAM and CALIOP) or the optical depth of stratospheric aerosols from sun photometer measurements (prior to 1978). As was noted previously (Arfeuille et al., 2013), the retrieval of SAGE V5.9 (or lower) is significantly different from SAGE V6.0 (or higher), and should no longer be used. The SAGE II algorithm team classified the algorithms used prior to V6.0 as poor in estimating the position where the sun tracker started losing the solar signal under heavily aerosol-laden conditions, with significant errors in both location of the sun. The effect was an unacceptable broadening of the layers with high extinction to much higher and lower altitudes, leading to a vertical smearing in the profile by several kilometers (2 – 5 km). For this record, we identified the issues in SAGE V5.9 (and prior), produced our aerosol data record based on SAGE V6, and Arfeuille et al. (2013) illustrated its performance for the case of the Pinatubo eruption period. While the results in Arfeuille et al. (2013) were still based on SAGE V6, in the present paper a version of the SAGE-3λ method is described, which is based on SAGE V7, although the aerosol products of both SAGE versions do not differ a lot. Furthermore, HALOE data, namely extinctions coefficients at 3.46 $\mu\mathrm{m}$, were used to further optimize the effective radii of the aerosol. We validate the results of SAGE-3λ by comparing with the AEC at the infrared channels of HALOE and CLAES-ISAMS. These channels mainly record absorption and much less scattering, and are thus largely proportional to the volume of aerosols (Arfeuille et al., 2013).

S1.1 SAGE II operational period (Oct 1984 – Aug 2005)

The SAGE (Stratospheric Aerosol and Gas Experiment) II instrument was launched aboard the ERBS (Earth Radiation Budget Satellite) in October 1984. The instrument used the solar occultation technique and measured attenuation of the solar radiation through the atmosphere. It provided profiles of AEC at four wavelengths (1020, 525, 452 and 386 nm) for 21 years, so far the longest time series of global satellite data on stratospheric aerosol (Thomason, 2012). The operational SAGE II data processing included estimated surface area density (SAD) beginning with the release of V6.2 (Thomason et al., 1997). It was later updated such that the coefficients used in the operational retrieval were weighted by measurement uncertainty, thereby

Table S1. Overview of the parameterizations used in REMAP for different time periods. More parameterizations are used concurrently, for periods, in which less data are available. The parameterizations are based on the whole duration of the respective multi-λ data set, i.e. 1984 – 2005 for SAGE II and 2017 – 2023 for SAGE III.

Time period	main data set	parameterizations used	multi-λ data sets
1960 – 1979	AOD from photometers (550 nm)	none, but modelling	AER output
1979 – 1981	SAGE I (1020 nm)	$r_{\text{eff}}(k_{1020})$, $\sigma(k_{1020})$	SAGE II (corrected with HALOE), SAGE II (above 20 km)
1982 – 1984	SAM II (1020 nm)	$r_{\text{eff}}(k_{1020})$, $\sigma(k_{1020})$	SAGE II (corrected with HALOE), SAGE II (above 20 km)
1984 – 2005	SAGE II (1020, 525, 452, 386 nm)	$r_{\text{eff}}(k_{1020})$	SAGE II (corrected with HALOE)
2006 – 2011	CALIOP (532 nm)	$r_{\text{eff}}(k_{532})$, $\sigma(k_{532})$	SAGE II (corrected with HALOE), SAGE II (above 20 km)
2017 – 2023	GloSSAC (1020, 525, 452, 386 nm)	$\sigma(k_{1020})^*$	SAGE III (above 20 km)

*SAGE III measures at 1022 nm

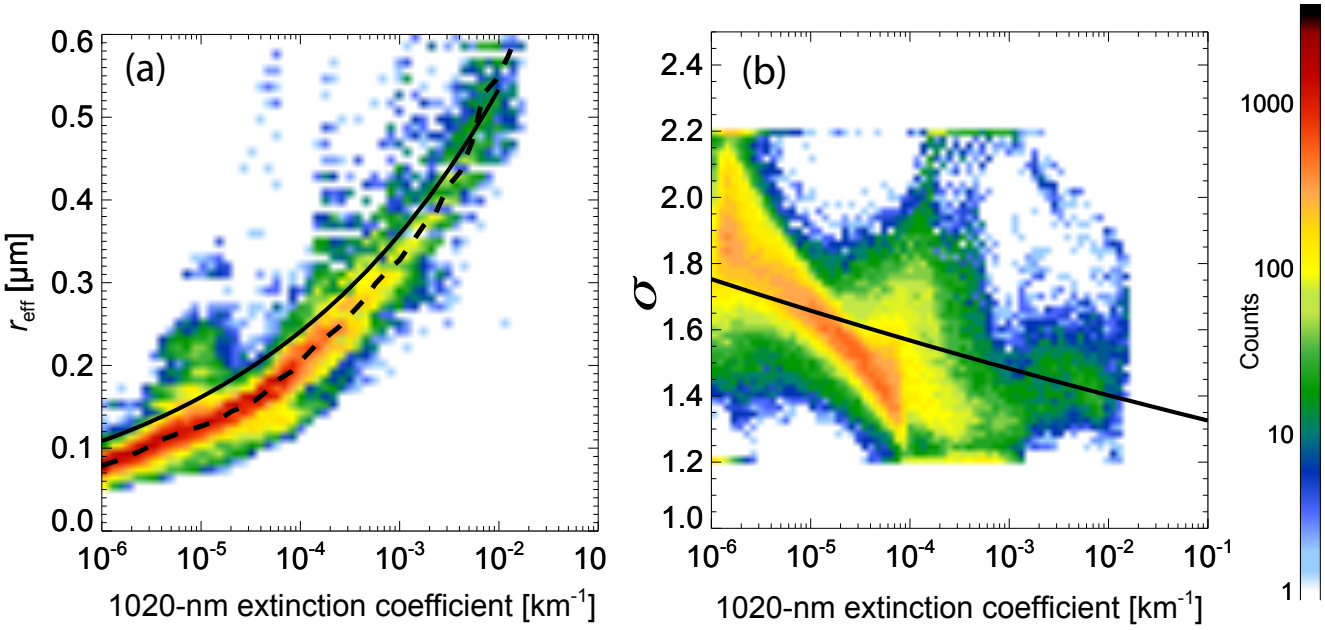

Figure S1. Effective radius and width of the stratospheric aerosol versus k_{1020} extinction coefficient.
(a) Occurrence of effective radii obtained from fitting n, r_m and σ simultaneously to the 4 wavelengths for all measurements above 20 km (without time interpolated or gap filled points). Dashed line: median value. Solid line: obtained by fitting in addition to the HALOE data at 3.45 µm (as used in this study).
(b) Correlation of the width of the log-normal distribution, σ, obtained from fitting n and σ simultaneously to the 4 wavelengths (>20 km, no filled points). r_m was obtained using the correlation of effective radius and the corresponding σ values. Solid line: best fit used, when extinction coefficient is available only at one wavelength.

moving the SAD-derivation dependence toward the 525 and 1020 nm channels, rather than the short wavelength channels that are generally less reliable (Thomason et al., 2008).

40

There are data gaps for the following reasons:

(a) at high latitudes, because sunrise or sunset are missing, typically during the polar winters;

(b) after strong volcanic eruptions, because the atmosphere with the volcanic aerosols becomes opaque for the occultation method, in particular in the lower stratosphere;

(c) when instruments did not function, e.g. because of maintenance work.

Thomason and Peter (2006) filled missing data during measurement gaps using temporal and/or spatial interpolation. During the Pinatubo period, a gap filling was performed based on ground station LIDAR data. In the present study, we additionally extrapolate to high latitudes based on the data of the last three available latitude bins.

For the SAGE-4λ and SAGE-3λ data sets we obtain the values for n, r_m and σ, which fit the extinction coefficients $(k_{1020}, k_{525}, k_{452}, k_{386})$ of SAGE II best at all 4 and 3 wavelengths, respectively (excluding k_{386} in the case of SAGE-3λ), wherever possible. Temperatures and relative humidities for the retrieval are taken from ERA-Interim to calculate the aerosol refractive index (Luo et al., 1996; Biermann et al., 2000). Here we used only data from 1991 as a yearly climatology.

For all data with at least 2 data points, we use the correlation for r_{eff} with k_{1020} (Figure S1a) given by

$$r_{\text{eff}} = 1.185\ \mu\text{m} \cdot (k_{1020}\ \cdot \text{km})^{0.173} \tag{1}$$

and retrieve n and σ.

For the periods, which were gap-filled with LIDAR data, only the AEC at 1020 nm is provided. Here, we use the correlations for r_{eff} with k_{1020} given by Eq. 1 and for σ with k_{1020} shown in Figure S1b given by:

$$\sigma = 1.254 \cdot (k_{1020}\ \text{km})^{-0.024263}. \tag{2}$$

The number density is then fitted to the only measurement. In Figure S2 we compare the measured and calculated AEC with the retrieved size distribution. The left panels show an unperturbed background case (November 1989), while the right panels show the results for a strongly volcanically perturbed period (April 1992).

During the background periods, the measured AEC at the wavelengths 1020, 525, 452 and 386 nm can be reproduced with excellent agreement. In volcanically perturbed periods, the agreement between the SAGE II data and the retrieval is worse (see panels (f) – (j) of Figure S2). However, the agreement is still reasonable, where more than 3 measurement data points exist (black contour). The gap-filled data can often not be well presented by a single-mode log-normal (SLN) size distribution during volcanic perturbations. In the present data set, the original SAGE II measurements are used to calculate a mean value for extinction when the number of data points exceeds 3. This approach could lead to an underestimation of the AEC, as the missing opaque data have a higher value (see Figure S2j) than the mean value of those, which are not opaque. In summary, during volcanically perturbed periods the SAGE-3λ and SAGE-4λ data sets have a higher uncertainty than during quiescent periods, with a potential low bias, in particular when the atmosphere becomes opaque.

S1.1.1 Data smoothing and use of HALOE extinctions.

To smooth the data during the period when SAGE II was operational and to enable the construction of the record before and after the SAGE II period, we use the effective radius r_{eff}, as it can be readily calculated from the mode radius r_m and width σ of the single-mode log-normal (SLN) distribution. The correlation of effective radii and k_{1020} is shown in Figure S1a, in which the dashed line is the median value. We use this median $r_{\text{eff}}(k_{1020})$ to first determine r_{eff} from k_{1020}, which allows to eliminate r_m, so that only the number density n and the half-width σ are left to be determined from the SAGE AEC data at all wavelengths. While this procedure reduces the noise in the data, the fitting quality using the $r_{\text{eff}}(k_{1020})$-correlation is only marginally worse than letting r_{eff} range freely as done in a *full retrieval*.

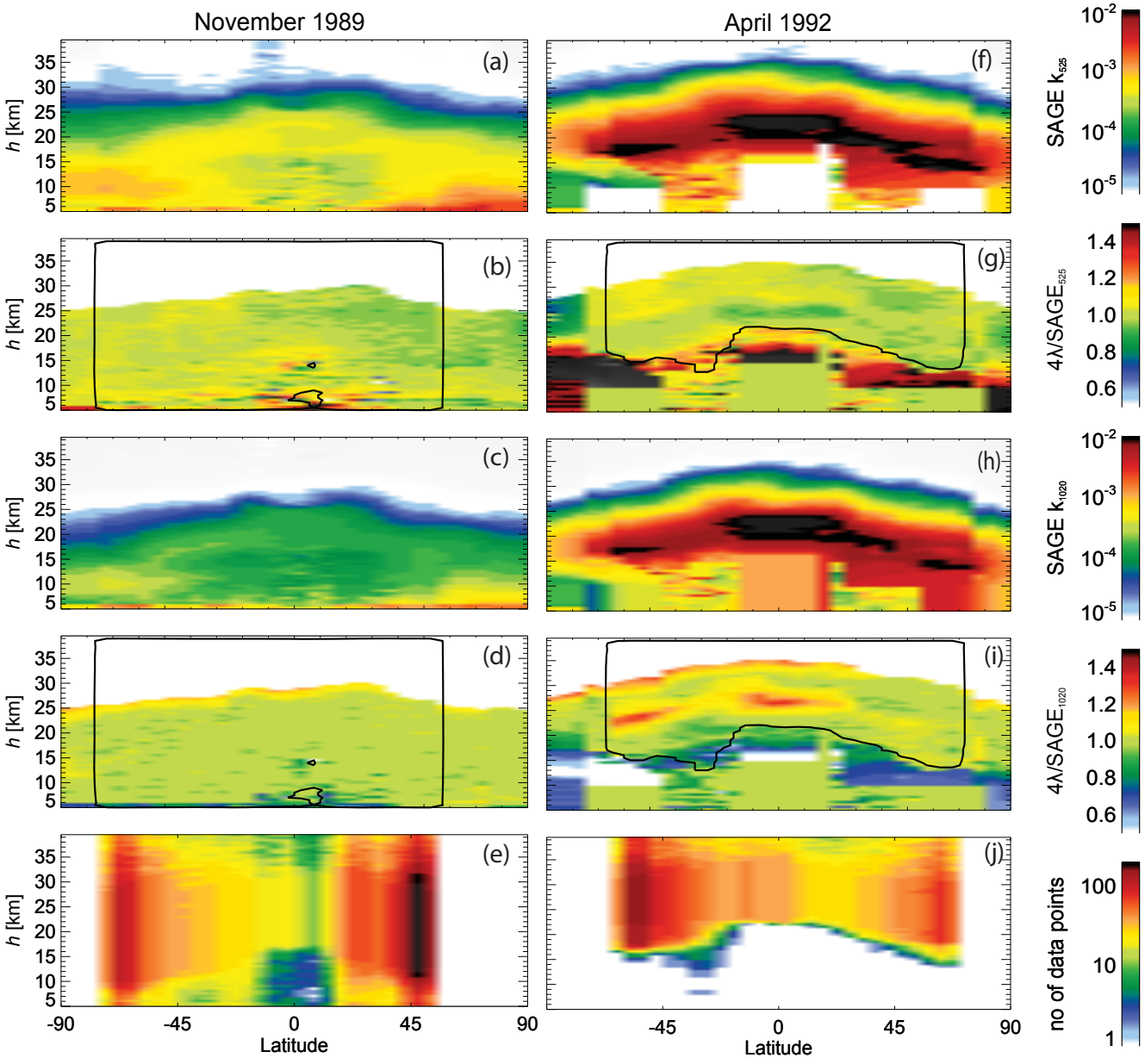

Figure S2. Comparison of monthly mean SAGE II extinction coefficients and extinction coefficients calculated from the retrieved size distributions. Left column: November 1989, volcanically unperturbed. Right column: April 1992, strongly perturbed. First row: k_{525} from SAGE II. Second row: ratio of k_{525} from SAGE-3λ over k_{525} from SAGE II. Third and fourth rows: same for 1020 nm. Fifth row: number of SAGE II data points. Black contours: regions where the number of SAGE data points is larger than 3.

The extinction coefficients of SAGE II are generally insensitive to very small particles (Thomason et al., 2008). This leads to significant uncertainties in the retrieved size distributions during periods with no or only low volcanic activity. In order to reduce uncertainty, we make use of additional extinction measurements at a wavelength with strong absorption, such as from the

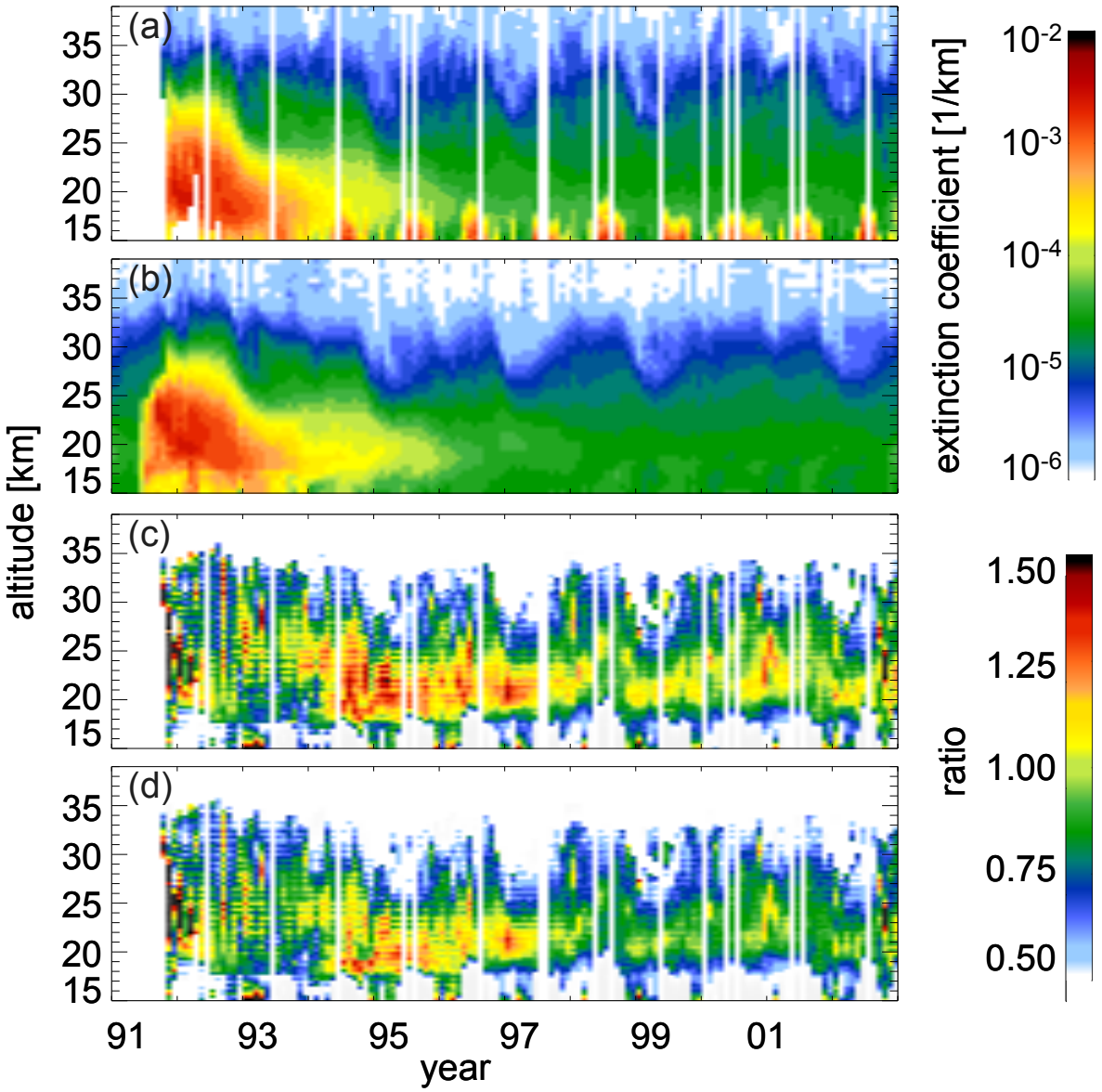

Figure S3. Comparison of extinction coefficients at 3.46 μm measured by HALOE with data computed using the retrieved size distributions. (a) HALOE data at 3.46 μm for 20 – 30° N. (b) Extinction coefficients at 3.46 μm from the SAGE-3λrecord using the adjusted r_{eff} (solid line in Figure S1a) including gap filling. (c) Ratio of SAGE-3λ with unadjusted r_{eff} (i.e. dashed line in Figure S1a) to HALOE extinctions at 3.46 μm (panel a). (d) Ratio of SAGE-3λ with adjusted r_{eff} (panel b and solid line in Figure S1a) over HALOE extinctions.

Halogen Occultation Experiment (HALOE), which provides a measure of the volume density of the aerosol (Thomason, 2012). The HALOE instrument measured extinctions at 2.80, 3.40, 3.46 and 5.26 μm. The HALOE AEC at 3.46 μm for altitudes >19 km was found to be most reliable (Thomason, 2012). Figure S3 shows the HALOE AEC and the comparison with the computed AEC at HALOE wavelength 3.46 μm using the size distributions retrieved from SAGE II data. The results using the unadjusted median effective radius (dashed line in Figure S1a) are shown in panel (c) of Figure S3. As mentioned above, the extinction

at 3.46 μm is mainly proportional to the volume density of aerosols. At moderate and low aerosol loading since 1994, using the unadjusted r_{eff} shown by the dashed line in Figure S1a leads to a smaller aerosol volume density than HALOE suggests. A better agreement of SAGE-[3/4]λ with HALOE data without significant loss of agreement with the original SAGE data can be achieved by adjusting the correlation of r_{eff} with k_{1020}, i.e. the solid line in Figure S1a, which is used for the present study, and is given by Eq. 1. The ratio of extinction coefficients at 3.46 μm computed with the adjusted r_{eff} to HALOE data is shown in Figure S3d. Now, maximum deviations from HALOE measurements are limited to 25 % in the period following 1994, as compared to 40 % with the unadjusted correlation.

S1.2 SAGE I (Jan 1979 – Nov 1981) and SAM II (Jan 1982 – Oct 1984) data

The SAGE (Stratospheric Aerosol and Gas Experiment) I and The Stratospheric Aerosol Measurement II (SAM II) data sets (McCormick et al., 1979) provide aerosol extinction coefficients at 1020 nm. Under these conditions, we use in addition to the correlation for r_{eff} (Eq. 1) the correlation of σ with the AEC at 1020 nm (Eq. 2) in the same manner as for the retrieval of gap-filled, LIDAR-based data during the SAGE II period. The only remaining unknown is then the aerosol number density n, which we calculate using the only measured extinction coefficient:

$$n = 1\ \text{cm}^{-3} \cdot \frac{k}{k\,(r_{\text{eff}}, \sigma)}. \tag{3}$$

Here, $k(r_{\text{eff}}, \sigma)$ is the calculated AEC of a SLN size distribution with an effective radius r_{eff}, half-width σ and number density of 1 cm^{-3} and k is the measured AEC. The correlation for σ with k at 1020 nm is shown in Figure S1b (using all SAGE II data above 20 km).

S1.3 CALIOP data (Jun 2006 – Dec 2011)

The Cloud-Aerosol LIDAR with Orthogonal Polarization (CALIOP) on the CALIPSO satellite (Cloud-Aerosol LIDAR and Infrared Pathfinder Satellite Observations) measured clouds and aerosol starting from June 2006 (Winker et al., 2007). The LIDAR instrument measures the backscattered signals of air molecules, aerosol and cloud particles. Coincident measurements by the GOMOS instrument (Global Ozone Monitoring by Occultation of Stars) of extinction coefficients are used to convert the backscatter coefficients measured by CALIOP to extinction coefficients at 532 nm (Vernier et al., 2011).

As with the other satellite instruments, the CALIOP data also need to be cleared from clouds, not only in the tropopause region, but also deep in the stratosphere, where polar stratospheric clouds (PSCs) may form during polar winters. In particular the Antarctic regularly develops PSCs. For the Antarctic, we extrapolate the data from the latitude band 55 – 60° S to the pole. In the Artic, PSCs are less critical, and we simply remove data points, which are obviously contaminated, then extrapolate from the last cloud-free data point to the pole. The subsequent retrieval is similar to the procedure for SAGE I and SAM II data, but for the CALIOP wavelength of 532 nm.

Similar to the occultation instruments, we first calculate the correlations of r_{eff} and σ with AEC at 532 nm (k_{532}). From stratospheric aerosol size distributions retrieved from the SAGE II data, we obtain the following correlations:

$$r_{\text{eff}} = 1.291\ \text{m} \cdot (k_{532}\ \text{km})^{0.20868} \tag{4}$$

$$\sigma = 1.8561 + 0.15467 \cdot \ln(k_{532}\ \text{km}) + 0.013536 \cdot \ln^2(k_{532}\ \text{km}). \tag{5}$$

The number density of aerosols n can then be readily calculated using Eq. 3 for wavelength 532 nm.

S1.4 Photometer data and model-based reconstruction 1960 – 1978

Stothers (2001) reconstructed the volcanic contribution to stratospheric aerosol optical depth based on the historical solar and stellar extinction data for the time period 1960 – 1978. Most of the ground stations with photometers are located in the latitude band 25 – 35 degrees. There is no information on the vertical distribution of the stratospheric aerosol. During this time two major volcanic eruptions occurred: Agung (8.3° S, 115.5° E) in March 1963 and Fuego (14.5° N, 90.9° W) in October 1974. In addition, there were at least five other tropical volcanic eruptions which also perturbed the stratospheric aerosol from 1965 to 1968 (Stothers, 2001).

In order to estimate the spatial and temporal evolution of volcanic eruption plumes of Agung and Fuego, we use the AER 2-D global model (Weisenstein et al., 2007). From the size distribution calculated from the AER 2-D model, we then estimate monthly mean optical depths at 550 nm in the Southern and Northern hemisphere in the latitude band 20 – 40°. Stothers (2001) provided only the perturbations of stratospheric aerosol due to volcanic activities, but no information on the quiescent background state. We use the SAGE II observations from 1996 – 2004 as a reference for the volcanically quiescent state. We subtract the optical depth for the quiescent state from the modelled optical depth. The obtained volcanic perturbation to the optical depth at 550 nm is then calibrated by means of a scaling factor to the photometer data from Stothers (2001). Finally, this scaling factor is applied to the entire hemisphere to obtain the spatial and temporal evolution of the volcanic eruptions of Agung and Fuego.

Similar to the procedure for CALIOP data, we use the extinction coefficients at 550 nm to retrieve the size distribution. The correlations of the effective radius and the width σ with the extinction coefficient at 550 nm k_{550} based on SAGE II data are given by the following equations:

$$r_{\text{eff}} = 1.291\ \mu\mathrm{m} \cdot (k_{550}\ \mathrm{km})^{0.2091}, \tag{6}$$

$$\sigma = 1.07 \cdot (k_{550}\ \mathrm{km})^{0.45951}, \tag{7}$$

which differ slightly from Eqs. 4 and 5 because of the marginally different wavelength. Again the number density can be calculated using Eq. 3, but for the wavelength 550 nm.

S1.5 Calculation of aerosol properties.

Analogous to main text.

S2 Effective radius profiles over Lauder, NZ

In addition to the SAD balloon profiles over La Réunion in the main text, such profiles are also available over Lauder NZ, some 25° further South, from 2019 to 2023. During this time frame, different states of the stratospheric aerosol are captured. Figure S4 shows the range of surface area density measurements from balloon ascents and descents (blue patch limited by two curves) and SAD retrieved from GloSSAC using REMAP (retrieval). While balloon measurements were taken in a single day within a few hours for both ascent and descent, GloSSAC uses mostly satellite data averaged over an entire month. The retrieval data also represents zonal averages over a 5 ° wide latitude band, while the balloons stayed within tens of kilometers of their launch point. The retrieval data agrees well with the balloon above some 13 km (e.g. 17 Nov 2020, 31 Aug 2021, 25 Nov 2023). Unperturbed conditions also come with the smallest SAD variability and smallest gaps between the balloon ascent and descent. On the other hand, on 27 Jan 2020 the balloon recorded elevated SAD from Australian bushfire smoke. The retrieval does not capture this at all, which is consistent with Figure 9 in the main text. The HTHH plume is first observed on 25 May 2022 by the balloon. For this month GloSSAC does not yet show the plume at this latitude (it appears in June), therefore

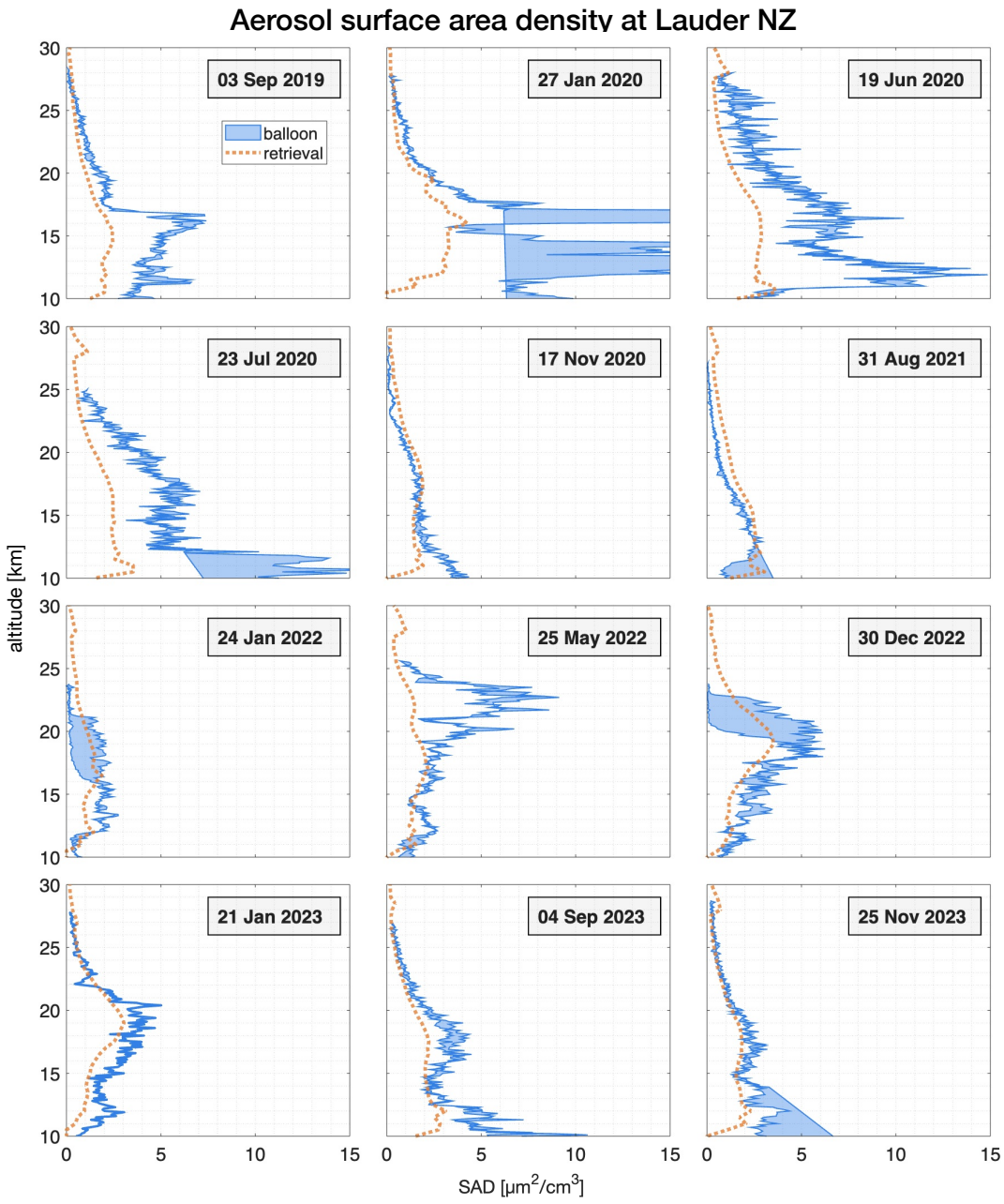

Figure S4. Comparison of balloon measurements and REMAP monthly mean values retrieved using GloSSAC. The filled blue patch is bounded by the ascent and descent balloon particle counter measurements. The data record both background conditions and perturbed aerosols on 27 Jan 2020 (smoke from Australian wildfires) and e.g. 25 May 2022 (sulfate particles from the Hunga Tonga Hunga Ha'apai volcanic eruption) over Lauder (NZ).

there is a large mismatch there. In the following 4 subplots the elevated SAD of the descending plume is well captured by the retrieval and in good agreement with the *in situ* balloon measurements. This comparison highlights the inability of REMAP

(and GloSSAC) to accurately capture non-volcanic aerosols and confirms the accuracy of not only retrieved AEC, but also derived variables like SAD.

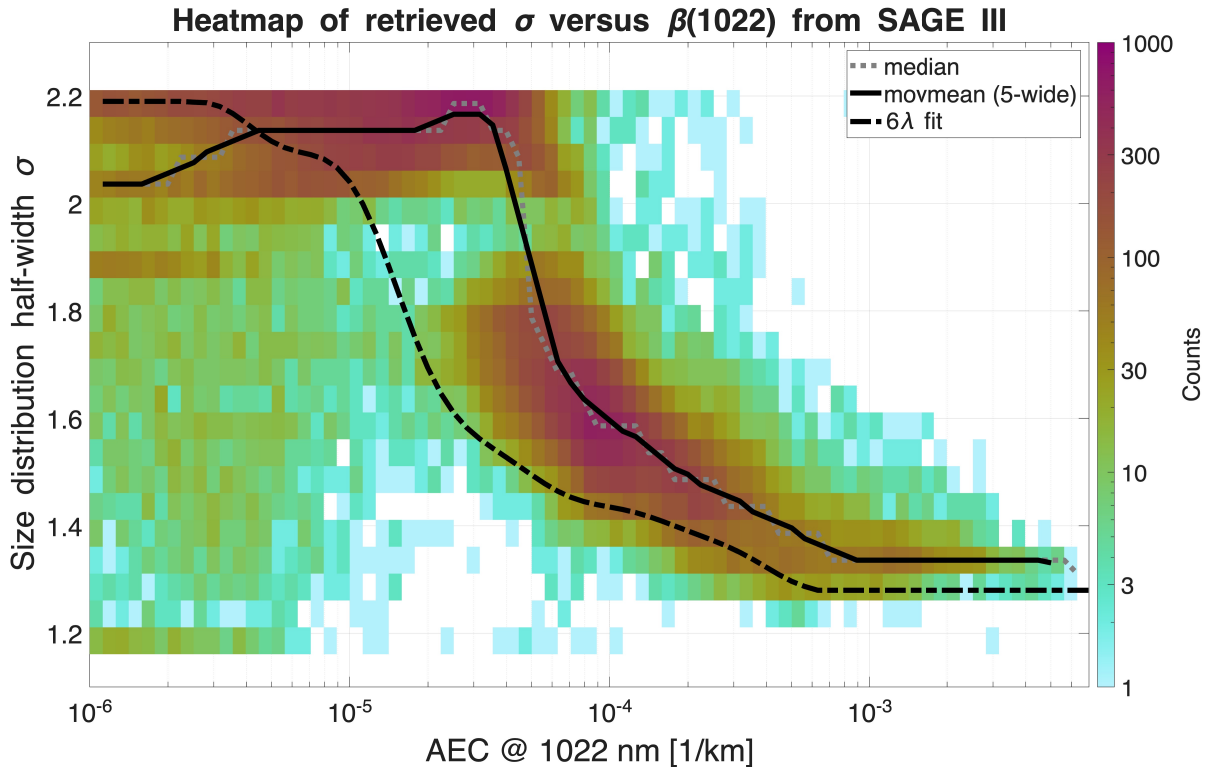

Figure S5. 2D histogram of all σ values retrieved from data of all 9 SAGE III wavelengths (June 2017 – December 2023, above 20 km) against their corresponding aerosol extinction coefficients. The dotted grey line shows the median value for every extinction coefficient bin, the solid black line shows the moving mean of the median at a width of 5 bins. The dot-dashed black line is the parameterization from a 6λ retrieval.

S3 Half-width parameterization

The parameterization in Figure S5 derived from SAGE III data is non-monotonic when using all 9 wavelengths for the retrieval of the size distribution. The cluster of σ-values at 2.2, which exceeds σ at lower AEC is unreasonable, since lower AEC are typically associated with a broader size distribution. We assume that these high values are an artefact of the method minimizing the fitting error between calculated and measured AEC, by adjusting the size distribution parameters. When there is a bias in the observational data, the method may force different parameters to their extremes (σ is constrained between 1.2 – 2.2) to try and get AEC similar to observations, which are impossible to fit well from a real, physical aerosol ensemble. The improved 6λ fit has the greatest difference to the moving mean in Figure S5 at this cluster and still significant difference throughout the higher AEC. This demonstrates the importance of wavelength channel quality assessment.

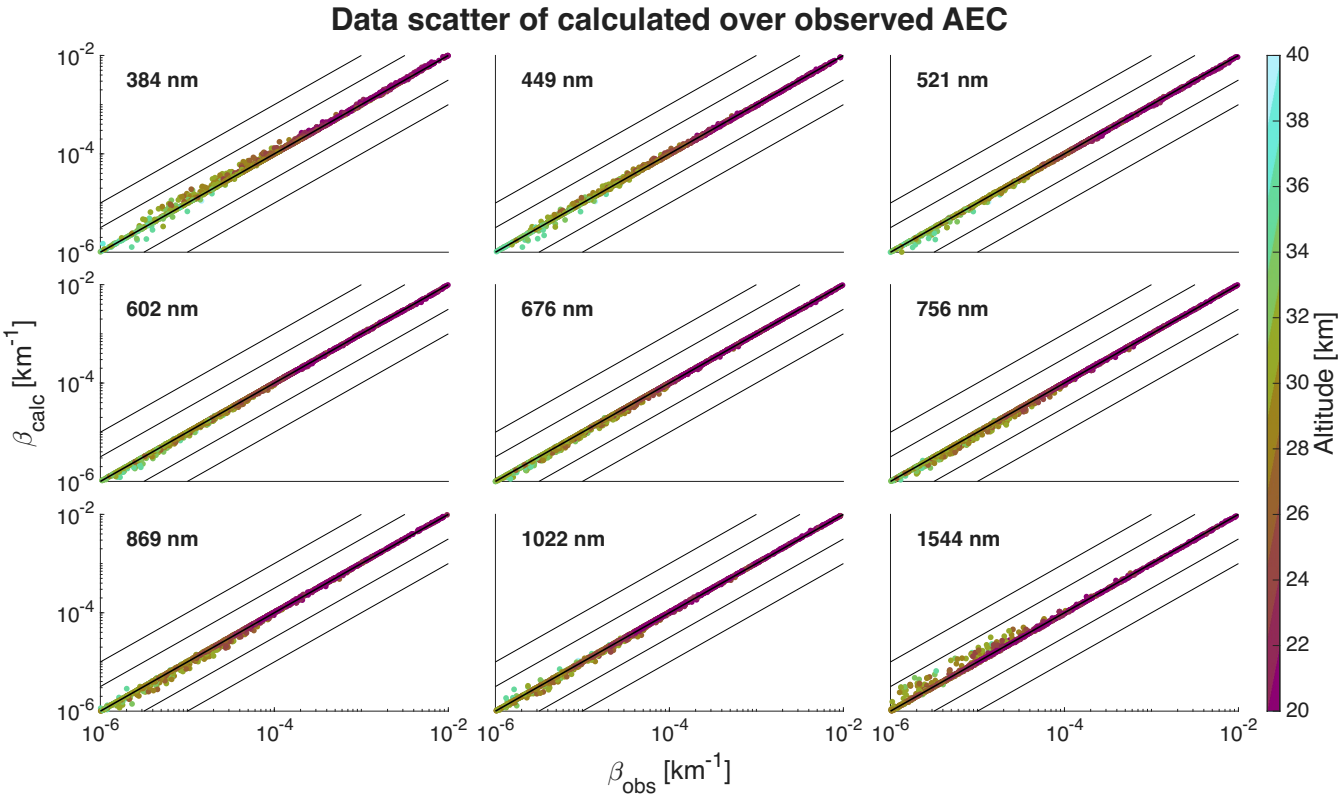

Figure S6. Scatter plots correlating calculated AEC β from OPC for all measurements above 20 km. The AEC were calculated for fitted bimodal log-normal size distributions (called β_{obs} here) and for retrieved unimodal log-normal size distributions (β_{calc} here). The colors are coded to the height of the measurement, with smaller AEC typically coming from greater heights. The differences between the two sets of AEC are very small.

S4 Single-mode log-normal assumption

REMAP so far has always exclusively used the parameters of a single-mode log-normal size distribution, to model the typical state of the stratospheric aerosol. But even for a multi-modal log-normal size distribution, the optical properties of the aerosol may be well recreated with a SLN size distribution. To test this we used the in situ optical particle counter (OPC) measurements above Laramie WY (Deshler, 2008). There are also size distributions reported with these measurements that have been fitted allowing for two log-normal modes. This means that in most cases the size distributions are bimodal, however, they can also only have a single mode if that best represents the OPC measurements. We select only the data above a height of 20 km and where the OPC measured on at least 9 channels (size bins). First, we calculated AEC with the (mostly) bimodal size distributions on the 9 SAGEIII wavelengths. Then we use these AEC data to perform a retrieval of SLN size distributions, the same way it is always done in REMAP. Once again, we can calculate the AEC from these new, now unimodal distributions. Figure S6 shows how these two sets of AEC compare. We call the AEC calculated from the bimodal OPC size distributions β_{obs} and the retrieved SLN AEC β_{calc}. There is great agreement for all channels with significant deviations from the 1:1-line only for small values that come from higher altitudes (>30 km). This demonstrates that REMAP can reliably recreate AEC, even though it only allows for a single aerosol mode. Still, the reduction from two modes to one retrieved mode yields good AEC. Figure S6 also shows how calculated AEC from a retrieval should ideally compare to AEC from observations without any bias in any of the wavelength channels. This is guaranteed here, because even the "observed" AEC follow from Mie theory.

References

Arfeuille, F., Luo, B. P., Heckendorn, P., Weisenstein, D., Sheng, J. X., Rozanov, E., Schraner, M., Brönnimann, S., Thomason, L. W., and Peter, T.: Modeling the stratospheric warming following the Mt. Pinatubo eruption: uncertainties in aerosol extinctions, Atmospheric Chemistry and Physics, 13, 11 221–11 234, https://doi.org/10.5194/acp-13-11221-2013, 2013.

Biermann, U. M., Luo, B. P., and Peter, T.: Absorption Spectra and Optical Constants of Binary and Ternary Solutions of H2SO4, HNO3, and H2O in the Mid Infrared at Atmospheric Temperatures, The Journal of Physical Chemistry A, 104, 783–793, https://doi.org/10.1021/jp992349i, 2000.

Deshler, T.: A review of global stratospheric aerosol: Measurements, importance, life cycle, and local stratospheric aerosol, Atmospheric Research, 90, 223–232, https://doi.org/https://doi.org/10.1016/j.atmosres.2008.03.016, 2008.

Luo, B., Krieger, U. K., and Peter, T.: Densities and refractive indices of H2SO4/HNO3/H2O solutions to stratospheric temperatures, Geophysical Research Letters, 23, 3707–3710, https://doi.org/10.1029/96GL03581, 1996.

McCormick, M. P., Hamill, P., Pepin, T. J., Chu, W. P., Swissler, T. J., and McMaster, L. R.: Satellite Studies of the Stratospheric Aerosol, Bulletin of the American Meteorological Society, 60, 1038–1046, http://www.jstor.org/stable/26219219, 1979.

Stothers, R. B.: Major optical depth perturbations to the stratosphere from volcanic eruptions, Journal of Geophysical Research: Atmospheres, 106, 2993–3003, 2001.

Thomason, L. W.: Toward a combined SAGE II-HALOE aerosol climatology: an evaluation of HALOE version 19 stratospheric aerosol extinction coefficient observations, Atmospheric Chemistry and Physics, 12, 8177–8188, https://doi.org/10.5194/acp-12-8177-2012, 2012.

Thomason, L. W. and Peter, T.: Assessment of stratospheric aerosol properties (ASAP), 2006.

Thomason, L. W., Poole, L. R., and Deshler, T.: A global climatology of stratospheric aerosol surface area density deduced from Stratospheric Aerosol and Gas Experiment II measurements: 1984–1994, Journal of Geophysical Research: Atmospheres, 102, 8967–8976, 1997.

Thomason, L. W., Burton, S. P., Luo, B.-P., and Peter, T.: SAGE II measurements of stratospheric aerosol properties at non-volcanic levels, Atmospheric Chemistry and Physics, 8, 983–995, https://doi.org/10.5194/acp-8-983-2008, 2008.

Vernier, J.-P., Thomason, L. W., Pommereau, J.-P., Bourassa, A., Pelon, J., Garnier, A., Hauchecorne, A., Blanot, L., Trepte, C., Degenstein, D., and Vargas, F.: Major influence of tropical volcanic eruptions on the stratospheric aerosol layer during the last decade, Geophysical Research Letters, 38, n/a–n/a, https://doi.org/10.1029/2011GL047563, 2011.

Weisenstein, D. K., Penner, J. E., Herzog, M., and Liu, X.: Global 2-D intercomparison of sectional and modal aerosol modules, Atmospheric Chemistry and Physics, 7, 2339–2355, 2007.

Winker, D. M., Hunt, W. H., and McGill, M. J.: Initial performance assessment of CALIOP, Geophysical Research Letters, 34, L19 803, https://doi.org/10.1029/2007GL030135, 2007.